Melting Point Depression Effect with CO_2 in High Melting Temperature Cellulose Dissolving Ionic Liquids. Modeling with Group Contribution Equation of State

Joana M. Lopes[1], Francisco A. Sánchez[2], S. Belén Rodríguez Reartes[2], Mª Dolores Bermejo[1*], Ángel Martín[1], Mª José Cocero[1]

[1] *High Pressure Process Group, Departmento of Chemical Engineering and Environmental Technology, University of Valladoid, Spain*

[2] *Planta Piloto de Ingeniería Química (PLAPIQUI-UNS-CONICET), Camino La Carrindanga Km 7, 8000 Bahía Blanca, Argentina.*

*mdbermejo@iq.uva.es

Abstract

Ionic liquids of the alkylmethylimidazolium chloride family are able to solubilize high amounts of cellulose and other natural polymers and have very good characteristics for their processing. Nevertheless, they present important disadvantages related to their high melting points and viscosities. Dissolution of carbon dioxide (CO_2) can reduce the melting point of these ionic liquids. In this work, the effect of pressurized carbon dioxide on the melting point depression of some ionic liquids able to dissolve biopolymers was experimentally determined using the first melting point method. Five different ionic liquids were studied using a high-pressure visual cell, up to a pressure of 10 MPa. The ILs studied were four ionic liquids with chloride anion coupled with 1-butyl-3-methylimidazolium cations: [C_4mim]$^+$, 1-ethyl-3-methylimidazolium, [C_2mim]$^+$, 1-allyl-3-methylimidazolium, [Amim]$^+$ and 1-(2-hydroxyethyl)-3-methylimidazolium, [C_2OHmim]$^+$ and one ammonium-based cation choline [$C_5H_{14}NO$]$^+$ combined with dihydrogen phosphate anion, [H_2PO_4]$^-$. Melting point depression effect observed for these groups of ionic liquids were around 10 K for chloride ILs and went as high as 33.2 K for choline dihydrogen phosphate. To correlate the melting point depression of imidazolium chloride ILs, parameters for the Group Contribution Equation of State (GC-EoS) of Skjold-Jørgensen for the liquid phase plus a fugacity expression for solid phases was employed. Experimental data used for the parameterization includes literature data of binary vapor-liquid, liquid-liquid and solid-liquid equilibria, and activity coefficients at infinite dilution. Melting point depression was calculated with an average deviation of 1.7 K (0.5%) and a maximum deviation of 4.3 K (1.3%).

1.   Introduction

Ionic liquids (ILs) are substances composed entirely of ions that generally are fluid around or below 100°C [1]. The unique physicochemical properties of ILs such as low vapour pressure [2], and high solvation ability to dissolve various organic and inorganic substances allows their use as green solvents in several applications. Furthermore, ionic liquids can be easily modified by changing the structure of the cations or anions and, thus also their properties.

One of the most promising application of ionic liquids is cellulose processing. Some ILs have been demonstrated to be highly effective solvents for the dissolution of cellulose in amounts as high as 25% in mass [3], sometimes even at room temperature [4]. Nevertheless the high viscosity of ILs which is greatly increased when they dissolve cellulose is the main limitation for their use in those processes. Imidazolium chlorides, acetates and alkylphosphates can dissolve high amounts of cellulose and other biopolymers, but recently acetates and alkylphosphates has been preferred due to their lower viscosities and melting points [4] caused by their asymmetrical cation and anions. The large size of the anions enlarges the distance between cation and anion, making the ionic interaction weaker. Thus, the imidazolium chlorides present a more regular packing and consequently high melting temperatures and viscosities. For these reasons, these ILs are sometimes set aside in cellulose processing, even though they are more effective than the others in hydrolysis [5] and avoid using strong acids in cellulose acylation reactions.

The melting process of ILs is governed by Van der Waals forces and electrostatic interaction forces and each one plays different roles for different kinds of ILs constituting a very complex behavior [6]. As Bourbigou et al. [7] reviewed, the length of the alkyl chain, the existence of H-bond and the presence of impurities are factors that influence parameters such as dielectric constant values or solvent polarity as well as the competition for the ions between the added species and the counter-ion. The anion Cl^- is a good H-bond acceptor and its probable location has been proposed closer to the $C(2)$ of the imidazolium ring. This provides higher charged density, symmetry and a more regular network. Therefore an increase of viscosity and high melting points is related to a growth in the cohesive forces via hydrogen bonding between the chloride and protons of the imidazolium ring. On the other hand, in the crystal structure of (2-hydroxyethyl)trimethylammonium dihydrogen phosphate,

2

[$C_5H_{14}NO$][H_2PO_4], also known as choline dihydrogen phosphate ([Cho][DHP]) a number of O-H···O hydrogen bonds and C-H···O interactions are present [8]. The high crystallinity gives to this IL an elevated melting point (392 K).

It is known that mixing an IL with molecular solvents allows decreasing its viscosity and its melting point can be decreased. The viscosity of ILs-solvent mixtures is mainly dependent on the mole fraction of added molecular solvents [9]. This is also possible when using carbon dioxide (CO_2) as a co-solvent, which has the advantages of being non-toxic, cheap, and can be easily separated of the IL by depressurization. ILs and CO_2 are considered to be a promising media for the development of "green" technology [10]. In biphasic mixtures IL-CO_2 at high pressure, CO_2 can dissolve significantly into the IL-rich liquid phase as well at moderate pressures as high as 75% in mol, but no ionic liquid dissolves in the gas phase [10,11]. The first example of CO_2-induced melting point depression (MPD) was reported by Kazarian et al. [12], who investigated an imidazolium salt, 1-hexadecyl-3-methylimidazolium hexafluorophosphate, [C_{16}mim][PF_6] with CO_2. They reported a MPD of 25 K with a CO_2 pressure of 70 bar. Scurto and Leitner tested [13] a quaternary ammonium salt tetra-*n*-butyl-ammonium tetrafluoroborate, [NBu_4][BF_4], and reported a solid-liquid transition temperature depression higher than 100K under 150 bar of CO_2. Later [14], they tested quaternary ammonium and phosphonium cations that showed strong depression as high as 80 K and 120 K. The method generally used was that of first melting point, with the exception of Serbanovic and coworkers that used a different method consisting in introducing a IL in a capillary tube inside a high pressure cell and increasing the temperature till the last solid particle is melted [15]. Selected results from MPD measurements on imidazolium and ammonium-based ILs found in literature are summarized in tables 1 and 2 respectively. In general imidazolium and pyridinium cations showed a much lower MPD in the range of 20 K than ammonium based ILs that can show melting MPD higher than 100 K.

Table 1. Summary of imidazolium-based ionic liquids normal melting point T_m (°C), CO_2 pressure (bar) and MPD (°C) found in literature.

Compound	T_m (K)	P_{CO2} (bar)	MPD (K)	Ref.
[C_{16}mim][PF_6]	348	70	25	[10]
[C_4mim][CH_3SO_3]	345	150	19.6	[11]
[C_4mim][Tosyl]	341	150	25.8	[11]
[C_4mim][Cl]	342	150	10.2	[12]
[C_2mim][PF_6]	333	147	35	[15]
[C_5O_2mim][PF_6]	316	20	20	[15]

Abbreviations: 1-Hexadecyl-3-methylimidazolium hexafluorophosphate, $[C_{16}mim][PF_6]$; 1-butyl-3-methylimidazolium methanesulfonate, $[C_4mim][CH_3SO_3]$; 1-butyl-3-methylimidazolium tolylate, $[C_4mim][Tosyl]$; 1-butyl-3-methylimidazolium chloride, $[C_4mim][Cl]$; 1-ethyl-3-methylimidazolium hexafluorophosphate, $[C_2mim][PF_6]$; 1-[2-(2-methoxyethoxy)-ethyl]-3-methylimidazolium hexafluorophosphate, $[C_5O_2mim][PF_6]$.

Table 2. Summary of ammonium-based salts normal melting point T_m (°C), CO_2 pressure (bar) and MPD (°C) found in literature.

Compound	T_m (K)	P_{CO2} (bar)	MDP (K)	Ref.
$[(C_2H_5)_4N][NTf_2]$	375	35	82	[11]
$[(C_4H_9)_4N][BF_4]$	429	150	120	[12]
$[(C_4H_9)_3(CH_3)N][CF_3SO_3]$	356	50	43	[12]
$[AB][CF_3SO_3]$	321	40	31	[12]
$[(C_4H_9)_4N][Tosyl]$	345	100	33	[15]

Abbreviations: Tetraethylammonium bis(trifluoromethylsulfonyl)imide, $[(C_2H_5)_4N][NTf_2]$; tetrabutylammonium tetrafluoroborate, $[(C_4H_9)_4N][BF_4]$; methyl tributylammonium trifluoromethanesulfonate $[(C_4H_9)_3(CH_3)N][CF_3SO_3]$; (S)-1-hydroxy-*N,N,N*-trimethylbutan-2-ammonium trifluromethanesulfonate, $[AB][CF_3SO_3]$; tetrabutylammonium tosylate, $[(C_4H_9)_4N][Tosyl]$.

The solubility of CO_2 in different ILs has been studied together with CO_2 induced MPD. Recently was published a study on ammonium-based ILs tested up to 150 bar was published [16]. The MPD reported was between 25 K and 120 K and the solubility between 0.57 and 0.8 (mole fraction) at 369 K. Nevertheless, no positive correlation was found between the magnitude of the melting point lowering and the solubility of the gas in each liquid. Melting point induced by CO_2 is minor in the case of methylimidazolium-based ILs as observed in Table 1.

In this work an experimental study of the MPD of various ionic liquids (solid at room temperature) was carried out in the presence of pressurized CO_2 up to 100 bar. MPD of imidazolium chloride ILs, were correlated using Group Contribution Equation of State of Skjold-Jørgensen and parameters were adjusted using literature data of CO_2 solubility in the ionic liquid $[C_4mim][Cl]$ available in literature [17] as well as activity coefficient at infinite dilution.

2. Experimental Section

2.1. Materials

The ionic liquids used in this work were 1-ethyl-3-methylimidazolium chloride, $[C_2mim][Cl]$, 1-allyl-3-methylimidazolium chloride, $[Amim][Cl]$, 1-butyl-3-methylimidazolium chloride, $[C_4mim][Cl]$, 1-(2-hydroxyethyl)-3-methylimidazolium chloride, $[C_2OHmim][Cl]$ and (2-hydroxyethyl) trimethylammonium dihydrogen phosphate, $[C_5H_{14}NO][H_2PO_4]$. The structure of these ILs is shown in Table 3, all of which were pur-

chased from Iolitec (Germany). The water contents were determined by Karl-Fischer cou-lometric titration (Mettler toledo C20 coulometric KF titrator). Carbon dioxide (99.5% pu-rity) was supplied by Carburos Metalicos (Spain) and was used without further purification.

Table 3. Summary of ILs experimental melting point depression (MPD) in pressurized CO_2, purity and water content

Abbreviation	Structure
[C2mim][Cl]	
[C4mim][Cl]	
[Amim][Cl]	
[C2OHmim][Cl]	
[Cho][DHP]	
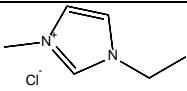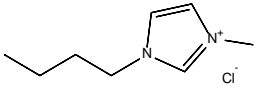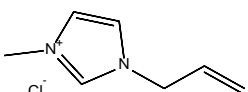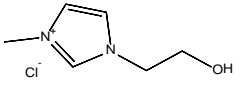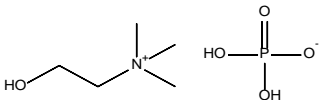
2.2. *Apparatus*

A schematic diagram of the equipment used for melting point measurements is shown in Fig. 1. The apparatus includes an optical cell (SITEC 740.2120) with an inner volume of 25 mL. Maximum operating temperature is 473 K and pressure is 500 bar. The cell has two opposite quartz windows. A lamp was used to illuminate one end of the view cell. The image was captured by a camcorder and displayed on the computer screen. The internal temper-ature of the cell was controlled by a PID temperature controller (OMRON E5GN) acting over an electrical jacket. The temperature was measured with a *K* type thermocouple with an accuracy of 1.5 K. The pressure was measured with a membrane relative pressure meter DESIN TPR 18/V2, with an accuracy of 0.2% span (0-400 bar) (accuracy 0.8 bar). The equip-ment and the methodology used has been described somewhere else [18].
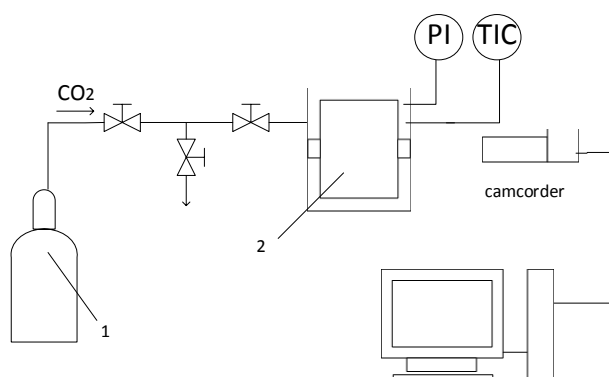
Figure 1. Scheme of the apparatus for melting temperatures measurements: 1, CO_2 supply; 2, optical cell.

2.3. Method

The experiment starts with a small amount of ionic liquid in a glass vial introduced in the optical cell. First the cell was keep at vacuum for 15 minutes in order to remove air and volatile impurities. Afterward, the cell was filled with CO_2 and pressurized up to the desired operating pressure. At fixed pressure, and after an equilibration time of about 15 min, the cell was gradually heated at a rate of 5 K/30 min until melting of the ionic liquid sample was observed with the camcorder. The melting point temperature of the ILs was measured when the surface starts to melt, according to the "First Melting Point" method. Each measurement was repeated 3 times to determine the standard deviation in measurements.

2.4. Differential scanning calorimetry

Differential scanning calorimetry (DCS) of the ILs was performed using a DSC 822e Mettler Toledo SAE, with a high sensibility ceramic sensor FSR5 whose characteristics are detailed in Table 4. During the analysis nitrogen of analytical quality was used as purge gas with a flow of 50 cm^3/min. Aluminum crucible standard, 40ul with pin (REF: ME-27331. from Mettler Toledo SAE) was used. Samples were weighted under nitrogen in a Balance Mettler. AT-261 with a precision of 0.01 mg. Temperature was increased from 298 to 423 K at 10 K/min.

Table 4. Characteristic of DCS sensor.

T Range (K)	Resolution (µW)	Enthalpy Range (mW)	Sensibility (µV/µW)
-123- 973	<0.04	± 350 (100 K)	15
		± 250 (300 K)	
		± 200 (700 K)	

3. Results and Discussion

3.1. Normal melting point and fusion enthalpies

Normal fusion temperatures and enthalpies of the ILs were determined by DSC and they are listed in Table 5. DSC curves are shown in Fig. s1 to s4 of supplementary information.

Table 5. DSC results measured in this work.

IL	T onset (K)	T peak (K)	ΔH [DSC] (kJ/mol)
[Amim][Cl]	315.75	324.95	-15.44 ± 0.06
[C$_4$mim][Cl]	335.45	341.35	-20.44 ± 0.09
[C$_2$OHmim][Cl]	360.35	363.35	-22.78 ± 0.12
[Cho][DHP] (Peak 1)	362.15	367.95	-12.957 ± 0.009
[Cho][DHP] (Peak 2)	391.85	395.55	-0.9586 ± 0.0008

Our results are compared to measurements of melting point and fusion enthalpies of other authors in Table 6. In general, important divergences are found in fusion enthalpy and melting temperature among the different authors: for [C$_4$mim][Cl], our fusion enthalpy is in the range of other author's values, while our melting temperature is also in the range but it is somehow lower than most literature values. In the case of [Amim][Cl] and [C$_2$OHmim][Cl] very few experimental values are available, existing great divergences among them, and our data present a higher melting temperature than other's author data, existing great divergences among them. In the case of [Cho][DHP], the DSC showed two peaks, being the fusion temperature reported in literature similar to the second peak reported [8].

Table 6. Comparison of different ILs normal melting points and fusion enthalpies

IL	T_m (K)	ΔH_{fus} (kJ/mol)	Method	Purity	Humidity	Reference
[C$_4$mim][Cl]	335.35	20.44 ± 0.09	DSC	99%	1092 ppm	This work
	338.1 ± 1		DSC	Not stated	Not stated	[19]
	341.94 ± 0.5		DSC			[20]
	341.95 ± 0.5	14.057 ± 0.46	DSC	>98%		[21]
	340.1 ± 2		Visual			[22]
	330.1 ± 1		DSC			[23]
	314.1 ± 4		DSC			[24]
	342.95 ± 0.5	25.5 ± 2.5	DSC		0.1% mas	[25]
	341.8 ± 0.5	21.7 ± 0.6	DSC			[26]
	340.1 ± 2		Visual			[27]
	340.1 ± 2		Visual	99%		[28]
	340 ± 2		Visual			[29]
[C$_2$mim][Cl]	370.1 ± 0.2	15.1 ± 0.6	DSC	99,80%	Not stated	[30]
	361.75 ± 0.5	15.35 ± 0.53	DSC		0,2% mass	[25]
	334 ± 82		DSC		<20 ppm	[31]

IL						
	360.7 ± 0.5	15.5 ± 0.5	DSC			[26]
	360 ± 1		Visual			[32]
	350 ± 1		Visual			[32]
	358.1 ± 4		Visual	99%		[28]
	360.75± 0.2	15.16 ± 0.6		99,6%	not detected	[33]
[Amim][Cl]	307.53	0.524	DSC			[34]
	290,15					[35]
	324.95	-15.44 ± 0.06	DSC	>98%	1332 ppm	This work
[C2OHmim][Cl]	333.95±2			Not stated	Not stated	[36]
	367.95	-22.78 ± 0.12	DSC	99%	723 ppm	This work
[Cho][DHP]	392	-	DSC	Not stated	Not stated	[8]
	395.55		DSC			This work

3.2. Melting point depression

Table 7 shows the melting temperatures at vacuum and at different pressures of CO_2. It is observed that the melting points observed at vacuum are similar in most cases to the onset temperature provided by the DSC measurement listed in Table 5, as it is expected when dealing with a first melting point method. Measurement was taken when the first melting signs where observed on the surface of the ionic salt. Fig. 2 shows images from the measurement of [Amim][Cl] and [C$_4$mim][Cl] melting points at 40 bar and 100 bar respectively.
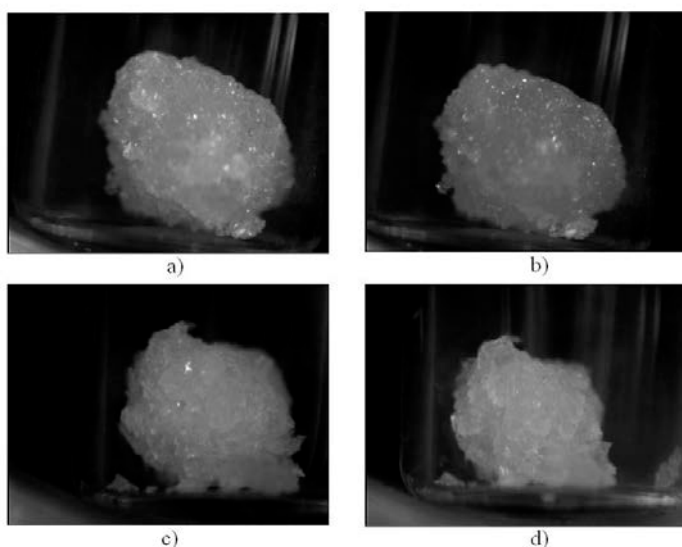
Figure 2. Pictures from experimental melting point measurements with pressurized CO_2 in the high pressure view cell: a) [Amim][Cl] at room temperature and vacuum; b) [Amim][Cl] at 40 bar and 313 K (observe the melted surface); c) [C$_4$mim][Cl] at 100 bar and 316 K; d) [C$_4$mim][Cl] at 100 bar and 325 K (observe the beginning of the melted surface.

Table 7. Experimental melting points at different pressures of CO_2

IL	P_{CO2} (bar)	T_m (K)

[Amim][Cl]	vacuum	311.4 ± 1.3
	10.6 ± 0.5	311.2 ± 0.6
	20.3 ± 0.2	309.3 ± 0.1
	30.9 ± 0.2	306.6 ± 0.6
	41.9 ± 1.4	303.5 ± 0.6
[C$_2$mim][Cl]	Vacuum	341.1 ± 0.6
	12.3 ± 1	341.3 ± 0.2
	20.2 ± 0.3	340.6 ± 0.1
	31.5 ± 1.1	340.6 ± 0.3
	42.1 ± 2.4	339.9 ± 0.2
	50.9 ± 1.1	338.0 ± 1.0
	100.7 ± 0.4	329.1 ± 0.5
[C$_4$mim][Cl]	Vacuum	335.3 ± 2.0
	11.7 ± 0.7	335.2 ± 0.1
	21.7 ± 0.1	333.1 ± 0.1
	41.2 ± 1.1	334.5 ± 0.5
	51.2 ± 1	332.3 ± 0.1
	100.5 ± 0.4	325.3 ± 0.1
[C$_2$OHmim][Cl]	Vacuum	349.3 ± 0.4
	11.2 ± 1.3	349.5 ± 0.2
	20.7 ± 0.4	349.1 ±0.5
	41 ± 0.4	348.5 ± 0.4
	52.3 ± 0.1	349.1 ± 1.7
	101.6 ± 1	343.5 ± 0.1
[Cho][DHP]	Vacuum	385.4 ±0.3
	20.3 ± 0.3	361.9 ± 1.7
	31 ± 1.2	360.0 ± 1.2
	40.9 ± 0.5	354.1 ± 0.5
	50.1 ± 0.1	352.6 ± 1.0
	100.6 ± 0.2	352.2 ± 0.3

Much larger MPD was found with [Cho][DHP] than with imidazolium chloride ionic liquids. This is consistent with literature data that shown much larger CO_2 induced MPDs for ammonium based ILs than for imidazolium ones [15] 33 K vs. 10 K of imidazolium based ILs at 100 bar. The first melting point observed at vacuum was near the onset temperature of the second DSC peak, considered the melting point in literature [8].

With regard to imidazolium chloride based ionic liquids at 40 bar, MPD is around 1 K, except for [Amim][Cl] for which is of 7.8 K, and more drastic MPD at pressures higher than 50 bar. At 100 bar MPD are much larger, of around 10 K in the following order: [C$_2$mim][Cl]> [C$_4$mim][Cl] >[C$_2$OHmim][Cl]. In literature it was also reported that for shorter alkyl chains in imidazolium based ILs, higher CO_2 induced MPD were observed [15]. The lowest one is observed in [C$_2$OHmim][Cl]. which could be attributed to the lower affinity of hydroxyl

group with CO_2 with respect to paraffine groups. This will be further discussed in the modeling section.

4. Thermodynamic modeling

The main objective of this section is to model the melting point decrease of the studied binary systems of CO_2 + alkylimidazolium chloride derivatives. Given the scarce information available of the ILs under investigation, we have adopted a group-contribution (GC) approach for the phase equilibrium modeling of these mixtures. The Group Contribution Equation of State (GC-EoS) originally developed by Skjold-Jørgensen [37] plus a mathematical expression for the solid fugacity has been applied to correlate and predict the melting temperature decrease of these mixtures. This model is based on Generalized van der Waals Theory with a local composition principle. In terms of the residual Helmholtz free energy, it can be expressed as a sum of free volume and attractive contributions:

$$\frac{A^{\mathrm{R}}}{RT} = \frac{A^{\mathrm{fv}}}{RT} + \frac{A^{\mathrm{att}}}{RT} \tag{1}$$

There are two contributions to the residual Helmholtz energy in the GC-EoS model: free volume and attractive. The free volume term follows the expression developed by Mansoori and Leland [38]:

$$\frac{A^{\mathrm{fv}}}{RT} = 3\frac{\lambda_1 \lambda_2}{\lambda_3}(Y-1) + \frac{\lambda_2^3}{\lambda_3^2}(Y^2 - Y - \ln Y) + n \ln Y \tag{2}$$

with

$$Y = \left(1 - \frac{\pi \lambda_3}{6V}\right)^{-1} \tag{3}$$

$$\lambda_k = \sum_{i=1}^{NC} n_i d_i^k \qquad (k = 1, 2, 3) \tag{4}$$

where n_i is the number of moles of component i, NC stands for the number of components, V represents the total volume, R stands for universal gas constant and T is temperature.

The following generalized expression is assumed for the hard sphere diameter temperature dependence:

$$d_i = 1.065655\, d_{ci}\left[1 - 0.12 \exp\left(\frac{-2\, T_{ci}}{3\, T}\right)\right] \tag{5}$$

where d_c is the value of the hard sphere diameter at the critical temperature, T_c, for the i-th component.

The attractive contribution to the residual Helmholtz energy, A^{att}, accounts for dispersive forces between functional groups. It is a van der Waals type contribution combined with a density-dependent, local-composition expression based on a group contribution version of the NRTL model [39]. Integrating van der Waals EoS, $A^{att}(T,V)$ is equal to $-a \cdot n \cdot \rho$ being a the energy parameter, n the number of moles and ρ the mole density. For a pure component a is computed as follows:

$$a = \frac{z}{2} q^2 g \tag{6}$$

where g is the characteristic attractive energy per segment and q is the surface segment area per mole as defined in the UNIFAC method [40]. The interactions are assumed to take place through the surface and the coordination number z is set equal 10 as usual. In GC-EoS the extension to mixtures is carried out using the two fluids model NRTL model, but using local surface fractions like in UNIQUAC [41] rather than local mole fractions. Therefore, the A^{att} for the mixture becomes

$$\frac{A^{att}}{RT} = -\frac{\frac{z}{2} \tilde{q}^2 g_{mix}}{RTV} \tag{7}$$

where $\tilde{q}$ is the total number of surface segments and g_{mix} the mixture characteristic attractive energy per total segments and are calculated as follows:

$$g_{mix} = \sum_{i=1}^{NG} \theta_i \sum_{j=1}^{NG} \frac{\theta_j \tau_{ij} g_{ij}}{\sum_{k=1}^{NG} \theta_{ik} \tau_{ik}} \tag{8}$$

and

$$\tilde{q} = \sum_{i=1}^{NC} \sum_{j=1}^{NG} n_i v_{ij} q_j \tag{9}$$

where v_{ij} is the number of groups of type j in molecule i; q_j stands for the number of surface segments assigned to group j; θ_k represents the surface fraction of group k;

$$\theta_k = \frac{1}{\tilde{q}} \sum_{i=1}^{NC} n_i v_{ik} q_k \tag{10}$$

$$\tau_{ij} = \exp\left(\alpha_{ij}\frac{\tilde{q}\,\Delta g_{ij}}{RTV}\right) \tag{11}$$

$$\Delta g_{ij} = g_{ij} - g_{jj} \tag{12}$$

g_{ij} stands for the attractive energy between groups i and j; and α_{ij} is the non-randomness binary damping factor. The attractive energy between unlike groups is calculated from the corresponding interactions between like groups:

$$g_{ij} = k_{ij}\sqrt{g_{ii}g_{jj}} \quad (k_{ij} = k_{ji}) \tag{13}$$

with the following temperature dependence for the energy and interaction parameters:

$$g_{ii} = g_{ii}^*\left[1 + g_{ii}'\left(\frac{T}{T_i^*} - 1\right) + g_{ii}''\ln\left(\frac{T}{T_i^*}\right)\right] \tag{14}$$

and

$$k_{ij} = k_{ij}^*\left[1 + k_{ij}'\ln\left(\frac{2T}{T_i^* + T_j^*}\right)\right] \tag{15}$$

where g_{ii}^* is the attractive energy and k_{ij}^* the interaction parameter at the reference temperature T_i^* and $(T_i^* + T_j^*)/2$, respectively.

4.1. *Group contribution approach for methylimidazolium chloride based ionic liquids*

In this work, the parameterization of a new group for methylimidazolium chloride based ILs ([-mim][Cl]) was performed. Fig. 3 illustrates the group decomposition for some ILs treated in this work. According previous to works [42,43], the corresponding IL molecule is divided in functional groups such as CH_3/CH_2 or CH_2OH, while the ionic contribution, i.e. cation + anion is kept as a single electroneutral group. Moreover, one methyl group attached to the imidazolium cation is kept within the whole ionic group in agreement with previous work for other imidazolium based ionic liquids [42,43].
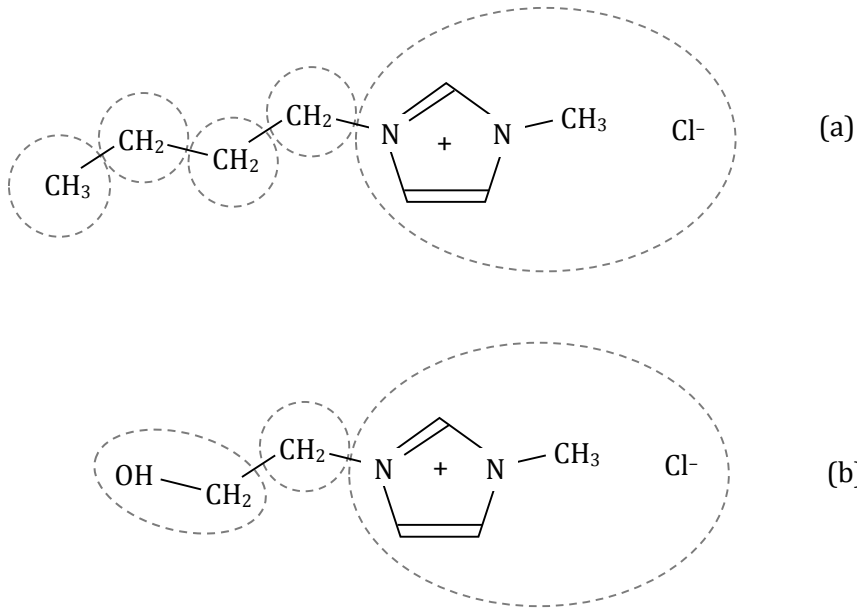
Figure 3. Group decomposition of some methylimidazolium chloride based ionic liquids treated in this work. **(a)** [C$_4$mim][Cl]; **(b)** [C$_2$OHmim][Cl].

4.1.1. Parameterization of the free-volume term

The free-volume term of the residual Helmholtz energy contains only one characteristic parameter, that is, the critical hard sphere diameter (d_c). Values for d_c are normally calculated from critical properties or by fitting the equation to *one single* vapor pressure data point (generally the normal boiling point). Since the main characteristic of ionic liquids is their negligible vapor pressure, this type of information is not available. Espinosa et al. [44] developed a correlation between the critical diameter d_c and the normalized van der Waals molecular volume (R_i) of high molecular weight compounds (*n*-alkanes, *n*-alkenes, saturated and unsaturated triacylglycerides, and alkylesters). This correlation was applied to calculate the critical diameter of ionic liquids from the estimated van der Waals volumes. Following a group-contribution approach, the normalized van der Waals volume of a compound, R_i, can be calculated as the sum of the constituent group volume parameters r_j:

$$R_i = \sum_{j=1}^{NG} v_{ij}\, r_j \tag{16}$$

Where v_{ij} is the number of groups j in molecule i. Similarly, the number of surface segments,

Q, of the i molecule can be obtained from its functional groups:

$$Q_i = \sum_{j=1}^{NG} v_{ij}\, q_j \tag{17}$$

13

Where q_j is the number of surface segments of group j. Although Eq. (16) and (17) are meant for molecules, they are also useful to calculate the reduced volume and surface of a larger group, as it is the case for the this new ionic group ([-mim][Cl]). Both r_j and q_j are defined as for the UNIFAC model [40] and Table 8 contains the values of r and q of the functional groups used in this work, all of which are calculated by means of the van der Waals volumes and surface areas given by Bondi [45]. The values of parameters R and Q for the [-mim][Cl] group have been calculated with its inner constituents shown in Fig. 4. The calculated normalized van der Waals volume and critical diameter of the ionic liquids studied in this work are reported in Table 9.

In order to evaluate the effective hard sphere diameter at a specified temperature, the GC-EoS requires an assigned value for the critical temperature, T_c, of the pure compound (see Eq. 5). In this work, the group contribution correlation of Valderrama and Rojas [46] has been applied to compute the values of the T_c of the ionic liquid studied in this work. All parameters referred to the free-volume term are listed also in Table 9.

Table 8. Normalized van der Waals segment volume and surface.

Group	r_j	q_j
CH$_3$	0.9011	0.848
CH$_2$	0.6744	0.540
CH=CH	1.1167	0.867
CH=CH$_2$	1.3454	1.176
CH$_3$-N	1.1865	0.940
CH=N	0.7329	0.324
Cl	0.7910	0.724
CH$_2$OH	1.2044	1.124
[-mim][Cl]	3.8271	2.855
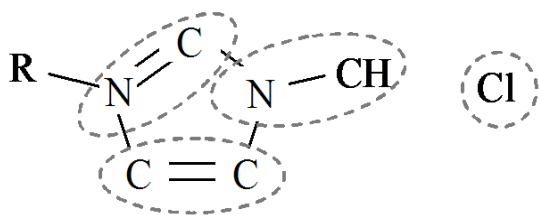
Figure 4. Groups contained within the [-mim][Cl] group for evaluating parameters $r_{[-mim][Cl]}$ and $q_{[-mim][Cl]}$.

Table 9. Pure component properties required for the GC-EoS.

IL	M	R_i	T_c [a] (K)	d_c [b] (cm/mol$^{1/3}$)	$T_{fus}/T_{tr,i}$ (K)	$\Delta H_{fus}/\Delta H_{tr,i}$ (J/mol)	v_t^L (cm³/mol)	v_t^S (cm³/mol)
[C$_2$mim][Cl]	146.6	5.4026	748.6	5.2194	361.75 [c]	15350 [c]	137.03 [a]	123.6 [g]
					353.15 [d]	-		
[Amim][Cl]	158.63	5.8469	770.7	5.3925	312.9 [d]	15444 [d]	136.0 [f]	116.3 [h]
[C$_2$OHmim][Cl]	162.6	5.7059	832.1	5.3925	349.7 [d]	22275 [d]	135.1 [a]	115.4 [h]
[C$_4$mim][Cl]	174.7	6.7514	789.0	5.7223	342.95 [c]	25540 [c]	160.6 [a]	137.3 [h]
					341.95 [e]	14050 [e]		
					335.48 [d]	20442 [d]		
[C$_8$mim][Cl]	230.8	9.4491	869.4	6.5742	–	–	–	–
[C$_{10}$mim][Cl]	258.8	10.7978	910.1	6.9464	311.17 [e]	30932 [e]	259.3 [a]	221.6 [h]
[C$_{12}$mim][Cl]	286.9	12.1466	951.5	7.2923	369.78/324.13/283.21 [e]	604/23580/1157 [e]	374.8 [a]	320.4 [h]

[a] Obtained using Valderrama and Rojas [46] group contribution method. [b] Calculated with Espinosa et al. [44] correlation. [c] Kick et al. [25]. [d] This work. [e] Domańska et al. [21]. [f] Wu et al. [47]. [g] Bolkan et al. [48]. [h] Goodman et al. [49].

4.1.2. Parameterization of the attractive term

For the parameterization of the attractive contribution, self and binary interaction parameters of the [-mim][Cl] must be set. Group interaction parameters for alkanes, alkene, alcohol and CO_2 groups have been taken from previous works [37,50,51]. The procedure to correlate pure and binary [-mim][Cl] parameters follows the method described by Breure et al. [42] which require activity coefficients at infinite dilution with normal alkanes. Up to our knowledge, this information is only available for some *n*-alkanes in 1-octyl-3-methylimidazolium chloride ([C$_8$mim][Cl]) [52]. To add robustness in the parameterization procedure, the mutual solubility of [C$_8$mim][Cl] with *n*-heptane and *n*-dodecane at 298 K reported by Letcher et al. [53] was added to the objective function reported by Breure et al. Thus, the objective function defined in this work is:

$$\text{O.F.} = w_\gamma^2 \sum_{i=1}^{NGam} \left(\frac{\gamma_{clc,i}}{\gamma_{exp,i}} - 1 \right)^2 + w_x^2 \sum_{i=1}^{NEq} \left(\frac{x_{clc,i}}{x_{exp,i}} - 1 \right)^2 \tag{18}$$

Where NGam and NEq are the number of activity coefficient and binary phase composition data points, γ are the activity coefficients, x represent phase compositions and w_u represents weights assigned to different kind of experimental data. Both weights have been set to 1.

The correlation procedure is identical to the one described by Breure et al. [42] in order to keep the number of adjustable parameters as low as possible. A linear temperature dependence for $g_{[-mim][Cl]}$ parameter was assumed ($g''_{[-mim][Cl]} = 0$); initially, all binary interaction parameters are assumed to be temperature independent and the mixture is considered to

15

behave as a regular solution ($k^*_{[-mim][Cl],i} = 1$; $k'_{[-mim][Cl],i} = 0$; $\alpha_{[-mim][Cl],i} = \alpha_{i,[-mim][Cl]}$ =0). This means that initially, the only adjustable parameters are self-interaction parameters: $g^*_{[-mim][Cl]}$ and $g'_{[-mim][Cl]}$. After this first correlation, self-interaction parameters are fixed and only binary interaction parameters $k^*_{[-mim][Cl],i}$, $\alpha_{[-mim][Cl],i}$ and $\alpha_{i,[-mim][Cl]}$ are used as adjustable parameters. Moreover, the non-randomness parameters are assumed to be the same within a family (for instance $\alpha_{[-mim][Cl],CH3} = \alpha_{[-mim][Cl],CH2}$, in accordance to previous works [37,42,43]). Last, a temperature dependence ($k'_{[-mim][Cl],i} \neq 0$) for the binary interaction parameter, or distinction between groups *may be* then introduced if needed to improve correlation. On the other hand, the parameterization of the interaction parameters between [-mim][Cl] and the resting groups included also binary vapor-liquid (VLE) and solid-liquid equilibria (SLE).

4.2. *Phase equilibrium equations*

Binary and ternary phase equilibrium calculation were performed by solving the isofugacity of the system between phases α and β at fixed temperature, T, and pressure, P,:

$$\hat{f}_i = x_{i,\alpha}\hat{\varphi}_{i,\alpha}P = x_{i,\beta}\hat{\varphi}_{i,\beta}P \qquad\qquad i = 1, NC \qquad (19)$$

where $\hat{f}_i$ is the fugacity of component *i* at equilibrium, and $x_{i,j}$ and $\hat{\varphi}_{i,j}$ represents the mole fraction and fugacity coefficient of component *i* in phase *j*. Fugacity coefficients of any component in the mixture are obtained by means of an equation of state. In this work, the GC-EoS model was applied to calculate the fugacity coefficients of all *fluid* phases. In case of solid-fluid equilibria, we follow the subcooled liquid reference state approach [54] assuming a pure solid phase for the heavy compound ($x_{IL,S} = 1$). For ILs treated in this work, many of the melting information to precisely evaluate the solid fugacity are not available. Up to our knowledge, no data about the heat capacity is avaible in open literature. With respect to density, experimental data of liquid [Amim][Cl] and solid [C_2mim][Cl] has been reported [47,48]. We have decided to: a) deprecate the change in the heat capacity during melting, which should not harm the solid fugacity calculation because the temperature ranges studied in this work are narrow in general; and b) to consider the change in volume during melting as constant. Thus, the expression proposed by Firoozabadi [54] for the fugacity of the solid becomes

$$f_{\text{IL}}^{S}(T,P) = f_{\text{IL}}^{L}(T,P) \exp\left[-\frac{\Delta H_{\text{fus}}}{R}\left(\frac{1}{T} - \frac{1}{T_{\text{fus}}}\right) - \frac{\Delta v_{\text{fus}}\,(P - P_{\text{fus}})}{R\,T} \right] \tag{20}$$

where f_{IL}^{S} and f_{IL}^{L} are the pure IL fugacity as a solid and liquid, respectively; T_{fus}, ΔH_{fus} and Δv_{fus} are the pure fusion temperature, and change in the enthalpy and volume of the pure solid and liquid phases.

For the modeling of SLE of binary mixtures which are at *atmospheric pressure*, it is possible to neglect the Δv_{fus}, since its contribution is minor at this condition. However, Δv_{fus} cannot be neglected for the calculation of the CO_2-induced MPD because pressure arises up to 100 bars in our experimental data (see Table 7). To overcome this limitation, we propose the following approach. First, estimate the liquid molar volume at 298 K of [C$_2$mim][Cl], [C$_4$mim][Cl] and [C$_2$OHmim][Cl] using the correlation of Valderrama and Rojas [46]. Although these ILs are solid at 298 K, we intend to obtain an approximation of the liquid density at melting point. Secondly, for the solid density of [Amim][Cl], [C$_4$mim][Cl] and [C$_2$OHmim][Cl], we propose to use the correlation of Goodman et al. [49]. These authors developed a correlation to estimate the saturated solid density (ρ_t^S) from the liquid density at the triple point (ρ_t^L). They proposed the following relation

$$\rho_t^{S} = 1.17\rho_t^{L} \tag{21}$$

from which it is possible to estimate the Δv_{fus} using the liquid or solid density information available. Values estimated using Eq. (21) are listed in Table 9, for the ILs studied in this work.

In principle, Eq. (20), together with the melting properties from Table 9 are enough for estimating the pure solid fugacity of the ILs in all binary mixtures with CO_2 studied in this work. Notwithstanding, Tables 7 and 9 highlights the existing dispersion regarding melting enthalpies of some imidazolium based ILs. Moreover, Eq. (21) provides only a rough estimation of the melting volume. Rodríguez Reartes et al. [55] faced a similar problem when dealing with the calculation of the solid-fluid equilibria of CO_2 with heavy compounds. These authors also state that errors in the constants ΔH_{fus}, Δv_{fus} will propagate to the calculated pure solid fugacity of the heavy compound, which also depends on the limitations of the selected EoS to calculate de liquid fugacity. In summary, Rodríguez Reartes et al. proposed

an alternative parameterization approach, keeping constant the prediction of the pure melting line. In such condition, liquid and solid fugacities are equal, which leads to the following expression from Eq. (20):

$$P = P_{\text{fus}} - \frac{\Delta H_{\text{fus}}}{\Delta v_{\text{fus}}}\left(1 - \frac{T}{T_{\text{fus}}}\right) = P_{\text{fus}} + C_1\left(1 - \frac{T}{T_{\text{fus}}}\right) \tag{22}$$

From Eq. (22) it is clear that if the relation $\Delta H_{\text{fus}}/\Delta v_{\text{fus}}$ (i.e. C_1) remains constant, the melting line of the pure compound is invariant. The pure solid fugacity may be then rewritten in terms of Δv_{fus} and C_1:

$$f_{\text{IL}}^S(T,P) = f_{\text{IL}}^L(T,P)\exp\left[-\frac{\Delta v_{\text{fus}}}{RT_{\text{fus}}}\left[C_1\left(1 - \frac{T}{T_{\text{fus}}}\right) - \frac{T_{\text{fus}}}{T}(P - P_{\text{fus}})\right]\right] \tag{23}$$

Rodríguez Reartes et al. [55] then proposed a parameterization strategy keeping constant C_1, (i.e., invariant pure melting line) while employing Δv_{fus} as an adjustable parameter. They show that perturbation in Δv_{fus} produces large and non-linear changes in the solid fugacity.

Thus, using a custom value while keeping constant the pure heavy compound melting line is a reasonable choice.

Last, is it worth to mention that given the dispersion found in T_{fus} and ΔH_{fus}, we decided to model each binary SLE data set with its specific values of T_{fus} and ΔH_{fus}. As an example, consider the binary systems involving [C$_4$mim][Cl] studied in this work. The data modeled in Fig. 8, measured by Domańska et al. [20], considered T_{fus} and ΔH_{fus} obtained by the same authors (see Table 9). On the other hand, MPD of [C$_4$mim][Cl] listed in Table 7, depicted in Fig. 10.b were modeled using melting properties obtained in this work (see Table 9).

The solution procedure applied in this work to solve the system of Eq. (19) is the *TP* flash with stability analysis as described by Michelsen [56,57]. On the other hand, the calculation of the solid-liquid-vapor lines required for the prediction of the melting depression follows the work of Rodríguez Reartes et al. [55]. They published a detailed algorithm for the calculation of binary solid-fluid-fluid equilibrium lines of asymmetric mixtures, like the ones treated in this work.

4.3. Modeling results and discussion

4.3.1. Mixtures of alkylimidazolium chloride ILs + hydrocarbons

The parameters obtained through correlation of experimental data are listed in Table 10. Table 11 reports the deviation between the GC-EoS model and experimental data, together with temperature and pressure ranges, references and number of experimental data points. As can be seen, binary interaction parameters $k^*_{[-mim][Cl],i}$ have been differentiated for i = CH$_3$ or CH$_2$ to improve correlation and prediction of experimental data, though no temperature dependence was introduced. On the other hand, the encountered binary dumping factors found to represent experimental data are asymmetric ($\alpha_{[-mim][Cl],i} \neq \alpha_{i,[-mim][Cl]}$) but not differentiation has been introduced between CH$_3$ and CH$_2$ groups. For i = CH=CH$_2$ and i = ACCH$_3$, only one single interaction parameter was correlated beacuse the only experimental data available are the activity coefficients reported by David et al. [52]. Deviations from experimental data listed in Table 11 show that the model presents activity coefficients at infinite dilution and mutual solubility of [C$_8$mim][Cl] + n-alkanes within the experimental error reported by the authors (3% for activity coefficients [52] and 0.006 for molar fractions [53]). The exceptions are the solubility of n-dodecane and n-hexadecane in [C$_8$mim][Cl], for which deviation obtained with the GC-EoS doubles the reported error. Fig. 5 depicts graphical results of this correlation for activity coefficients. Fig. 6 shows the predictions of the ternary phase equilibria of [C$_8$mim][Cl] + benzene + a n-alkane. The GC-EoS follows qualitatively the experimental tie-lines for intermediate compositions, founding little better results for n-dodecane than for n-heptane.

Table 10. New GC-EoS parameters for the [-mim][Cl] group.

Pure group parameter						
Group	q	T^*(K)	g^*(atm cm^6/mol^2)	g'	g''	Source
[-mim][Cl]	2.855	600.0	1844397	-0.1552	0	LLE of nC$_7$ or nC$_{12}$ at 298 K + γ_∞ of nC$_5$ & nC$_8$ + [C$_8$mim][Cl]

Binary interaction parameters						
Group		k^*_{ij}	k'_{ij}	α_{ij}	α_{ji}	Source
i	j					
[-mim][Cl]	CH$_3$	0.8215	0	-0.7577	-0.2539	LLE of nC$_7$ or nC$_{12}$ at 298 K + γ_∞ of nC$_5$-nC$_8$ + [C$_8$mim][Cl]
	CH$_2$	1.0838	0	-0.7577	-0.2539	
	CH=CH$_2$	0.7850	0	0	0	γ_∞ of 1-heptene + [C$_8$mim][Cl]
	CO$_2$	1.0409	0.1509	-1.4439	0.4677	Bubble pressures of CO$_2$ + [C$_4$mim][Cl]
	ACH	0.8620	0.0271	0.6717	1.4377	LLE at 298K + γ_∞ of benzene + [C$_8$mim][Cl]
	ACCH$_3$	0.9310	0	0	0	γ_∞ of toluene + [C$_8$mim][Cl]
	CH$_2$OH	1.0260	0	0.4148	-4.4988	SLE of C$_2$OH & C$_{12}$OH + [C$_4$mim][Cl].

Table 11. Model deviations of experimental data of correlated and predicted data points.

Compound		T (K)	P (bar)	ARD%(γ)		No exp points	Source
(1)	(2)						
Activity coefficient							
[C$_8$mim][Cl]	*n*-Pentane	298, 308, 318	1.01	3.0*		3	[52]
	n-Hexane	298, 308, 318	1.01	2.5		3	[52]
	n-Heptane	298, 308, 318	1.01	4.9		3	[52]
	n-Octane	298, 308, 318	1.01	2.6*		3	[52]
	1-Hexene	298, 308, 318	1.01	1.1		3	[52]
	1-Heptene	298, 308, 318	1.01	2.0*		3	[52]
	1-Octene	298, 308, 318	1.01	1.7		3	[52]
	Benzene	298, 308, 318	1.01	3.6*		3	[52]
	Toluene	298, 308, 318	1.01	2.8*		3	[52]

Binary liquid-liquid & SC fluid-liquid equilibria

Compound		T (K)	P (bar)	AAD (ARD%) of x_{ij}		No exp points	Source
				(1) in (2)	(2) in (1)		
[C$_8$mim][Cl]	*n*-Heptane	298	1.01	1.4E-3 (20)*	7.7E-3 (12)*	1	[53]
	n-Dodecane	298	1.01	6.2E-3 (65)*	1.2E-2 (49)*	1	[53]
	n-Hexadecane	298	1.01	5.9E-3 (62)	1.6E-2 (87)	1	[53]
	Benzene	298	1.01	1.5E-4 (2.1)*	1.6E-2 (2.3)*	1	[53]
[C$_4$mim][Cl]	CO$_2$	353, 373	24-360	-	2.0E-2 (7.7)*	19	[17]
		358,363,368	26-340	-	2.0E-2 (7.6)	27	[17]

Solid-liquid equilibria

Compound		T (K)	P (bar)	(1) in (2)	(2) in (1)	No exp points	Source
[C$_2$mim][Cl]	[C$_4$mim][Cl]	318-360	1.01	2.8E-2 (4.0)	3.5E-2 (4.8)	18	[25]
[C$_4$mim][Cl]	Etanol	298-342	1.01	2.4E-2 (3.5)*	-	29	[20]
	1-Butanol	273-342	1.01	0.17 (25)	-	12	[20]
	1-Hexanol	285-342	1.01	7.6E-2 (15)	-	32	[20]
	1-Octanol	273-342	1.01	8.1E-2 (8.1)	-	15	[20]
	1-Decanol	279-342	1.01	0.13 (130)	1.4E-2 (1.4)	23 / 3	[20]
	1-Dodecanol	286-342	1.01	2.6E-2 (2.6)*	2.3E-2 (2.6)	26/5	[20]
[C$_{10}$mim][Cl]	Etanol	276-311	1.01	6.9E-2 (12)	-	13	[58]
	1-Butanol	275-311	1.01	9.6E-2 (20)	-	22	[58]
	1-Hexanol	277-311	1.01	0.16 (41)	-	17	[58]
	1-Octanol	292-311	1.01	0.22 (57)	-	15	[58]
	1-Decanol	277-311	1.01	0.28 (144)	-	17	[58]
	1-Dodecanol	297-311	1.01	0.39 (183)	-	19	[58]
[C$_{12}$mim][Cl]	*n*-Octane	322-370	1.01	0.28 (74)	-	29	[59]
	n-Decane	323-370	1.01	0.25 (49)	-	25	[59]
	n-Dodecane	324-370	1.01	0.36 (124)	-	20	[59]
	Benzene	291-370	1.01	0.12 (23)	-	17	[59]
	Etanol	274-370	1.01	6.2E-2 (9.2)	-	26	[60]
	1-Butanol	276-370	1.01	7.9E-2 (12)	-	26	[60]
	1-Hexanol	273-370	1.01	0.17 (14)	-	34	[60]
	1-Octanol	273-370	1.01	9.4E-2 (22)	-	37	[60]
	1-Decanol	279-370	1.01	0.24 (157)	1.1E-2 (1.1)	38/4	[60]
	1-Dodecanol	296-370	1.01	0.37 (545)	1.3E-2 (1.3)	50/3	[60]

* Data included in parameterization procedure.
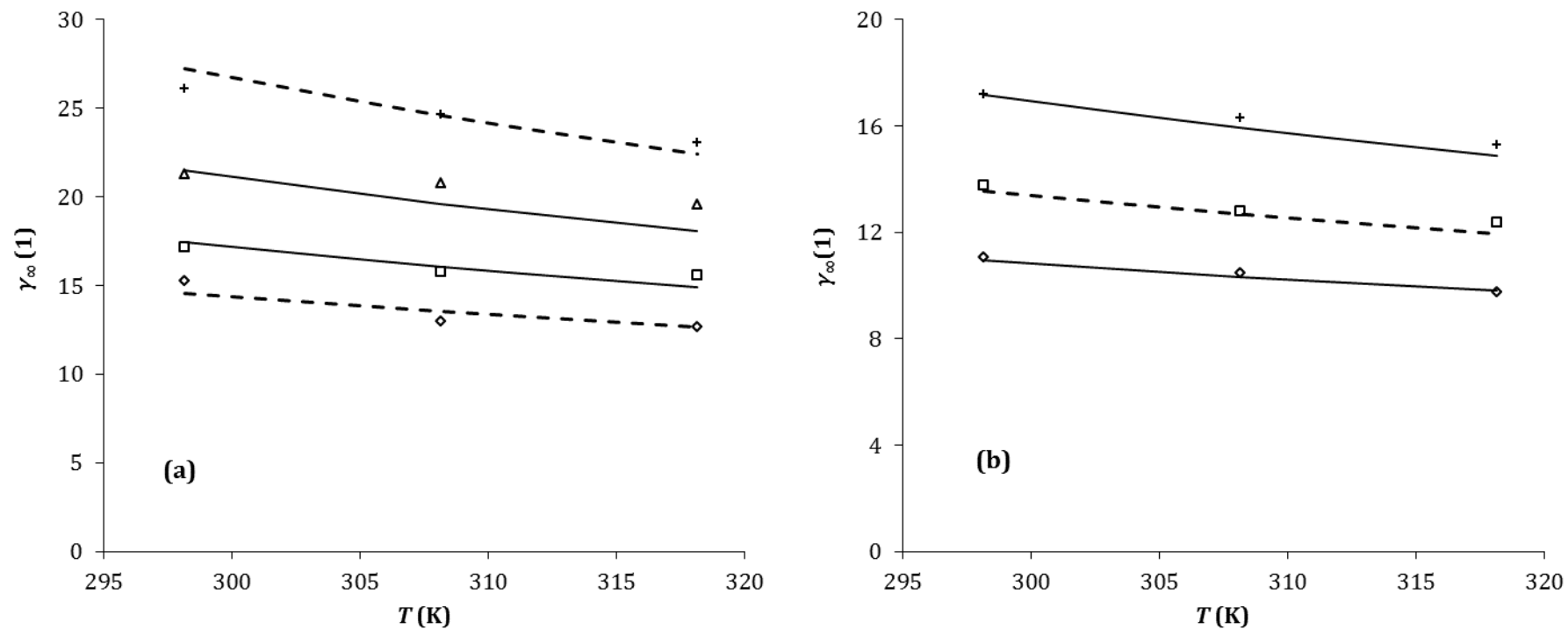
Figure 5. Activity coefficients at infinite dilution of hydrocarbons (1) in [C$_8$mim][Cl] (2) [52]. **(a)** ($\diamondsuit$) n-Pentane, ($\square$) n-hexane, ($\triangle$) n-heptane and (+) n-octane. **(b)** ($\diamondsuit$) 1-Hexene, ($\square$) 1-heptene and ($\triangle$) 1-octene. Dashed and solid lines: correlation and prediction using GC-EoS model, respectively, with parameters of Tables 9 and 10.
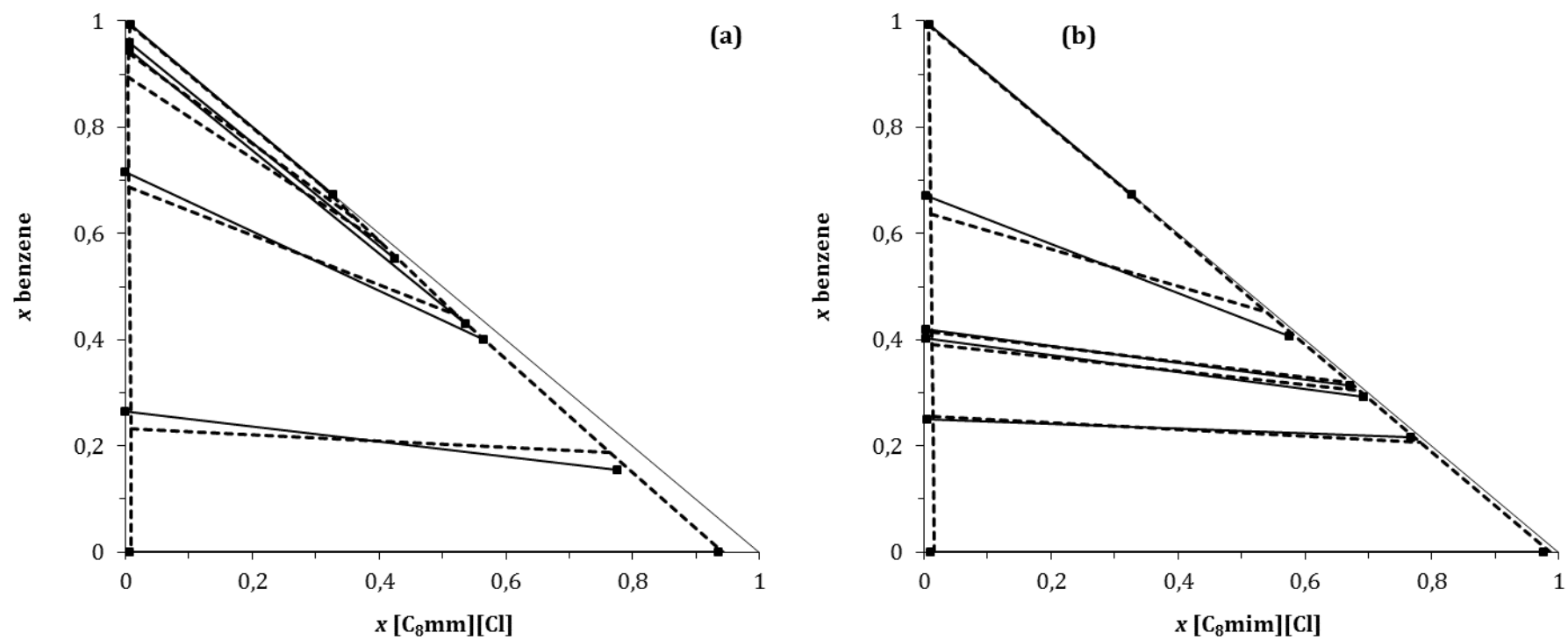
Figure 6. Prediction of the liquid-liquid equilibria of the ternary system [C$_8$mim][Cl] + benzene + *n*-alkane at 298 K. **(a)** *n*-Heptane; **(b)** *n*-dodecane. Symbols and solid lines represent experimental tie-lines [53], while the dashed lines are GC-EoS predictions.

Solid-liquid equilibria of [C$_{12}$mim][Cl] with alkanes deserves a special mention. This data type is an interesting challenge, since all interaction parameters are now fixed. Moreover, the phase equilibria of [C$_{12}$mim][Cl] presents polymorphism, showing pure solid-solid (SS) phase transitions. This is an important implication in the pure and mixture phase behavior, since the change in enthalpy of the first SS transition, $\Delta H_{tr,1}$, is much greater than ΔH_{fus} (see Table 9). Thus, specifically for the binary SLE data involving this compound, the following expression has been employed to model the fugacity of the solid phase:

$$f_{IL}^{S}(T,P) = f_{IL}^{L}(T,P) \exp\left[-\frac{\Delta H_{fus}}{R}\left(\frac{1}{T}-\frac{1}{T_{fus}}\right) - \sum_{i=1}^{NT(T)} \frac{\Delta H_{tr,i}}{R}\left(\frac{1}{T}-\frac{1}{T_{tr,i}}\right)\right] \qquad (24)$$

where NT(T) is the number of SS transitions present between T and T_{fus}, and $T_{tr,i}$ and $\Delta H_{tr,i}$ are the temperature and enthalpy of the SS transition. Eq. (24) is basically the same as presented by Domańska et al. [60], but deprecating the specific heat change. Fig. 7 shows the prediction of the SLE of [C$_{12}$mim][Cl] + n-octane and n-dodecane, using Eq. (24) for the pure [C$_{12}$mim][Cl] solid fugacity. The model predictions depicted by lines follow qualitatively the experimental data presented by Domańska et al. [59]. These authors reported the occurrence of a liquid-liquid split in a narrow composition region for the [C$_{12}$mim][Cl] + n-dodecane binary system. On the other hand, the GC-EoS predicts a wide liquid-liquid split for the three binary systems studied by Domańska et al. [59]. However, the experimental data follows an extremely flat tendency with an almost constant phase transition temperature, which may indicate a phase split not found because of the presence of SLE.
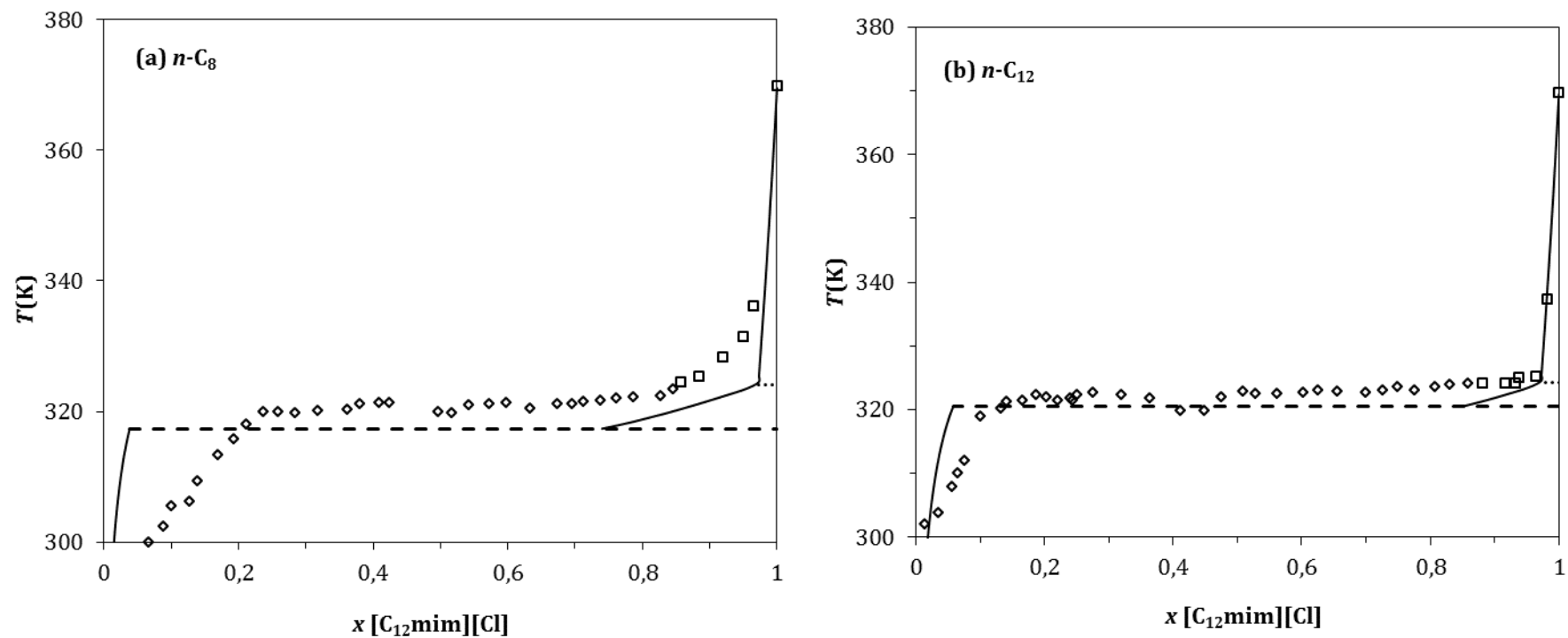
Figure 7. Solid-liquid equilibria of the system [C$_{12}$mim][Cl] + **(a)** *n*-octane and **(b)** *n*-dodecane. Experimental SLE data at atmospheric pressure taken from Domańska et al. [59]. Symbols represent experimental data of liquid + solid α (□) or solid β (◇). Lines represent GC-EoS prediction of SLE (solid), SSLE (dotted) and SLLE (dashed). Notice that the [C$_{12}$mim][Cl] fugacity as a pure solid was calculated by means of Eq. (24)

4.3.2. Mixtures of alkylimidazolium chloride ILs + alcohols

Experimental binary SLE data of alcohols with alkylimidazolium chloride based ILs is vast. The group of Domańska et al. have published an extensive study of SLE of the homologue series of n-alcohols with [C$_4$mim][Cl] [20], [C$_{10}$mim][Cl] [58] and [C$_{12}$mim][Cl] [60]. Moreover, Domańska et al. [21] measured the mutual solubility of 1-octanol + [C$_8$mim][Cl]. Table 11 lists all deviations of our modeling results from experimental data, which includes all SLE found, while Fig. 8 exemplify the correlation and predictions of the SLE of selected alcohols + ILs. LLE experimental data of 1-octanol + [C$_8$mim][Cl] were excluded from Table 11 because the model predicts one single phase for this system at experimental conditions studied in [20,21,58,60]. The experimental data reported shown a complex behavior, which is a challenge to any group-contribution thermodynamic model. For example, according to measured data, 1-octanol + [C$_4$mim][Cl] and [C$_{12}$mim][Cl] show complete miscibility in the liquid phase. However, as previously mentioned, the experimental data of the binary system 1-octanol + [C$_8$mim][Cl] present a phase split at the same temperature regions [21]. Moreover, the SLE of the binary 1-octanol + [C$_{10}$mim][Cl] reported by Domańska et al. [58] presents a flatness in temperature, typical of liquid phase splits (see Fig. 8.b). This non-linear transition of the mixture behavior when changing the length of the alkyl chain in the IL is not possible to be represented with a model such as the GC-EoS. The only difference between these compounds within the GC-EoS framework is the number of CH$_2$ in the IL and thus, the prediction of the phase behavior of mixtures of homologue series tends in general to be monotonic. A better approach could be to employ an association contribution to the Helmholtz free energy in Eq. (1) as it is done in the GCA-EoS model of Gros et al. [61], however, this is beyond the scope of this work. Given the limitations of the model to properly represent all analyzed experimental , we proposed the following approach: we selected some binary systems to be employed for the correlation of the experimental data, generating different sets of parameters. Then, the final set of parameters was selected between the different predictions achieved of the MPD of [C$_2$OHmim][Cl] in compressed CO$_2$. Nevertheless, this information was not included in the objective function defined in Eq. (18). The selected set of parameters were the result of the correlation of the SLE of [C$_4$mim][Cl] + ethanol and [C$_4$mim][Cl] + 1-dodecanol. Notice that groups [-mim][Cl] and CH$_2$OH are more concentrated in the mixture when the shorter the alkyl chain is (i.e., [C$_4$mim][Cl] + ethanol binary system), where less *noise* from other groups is present.
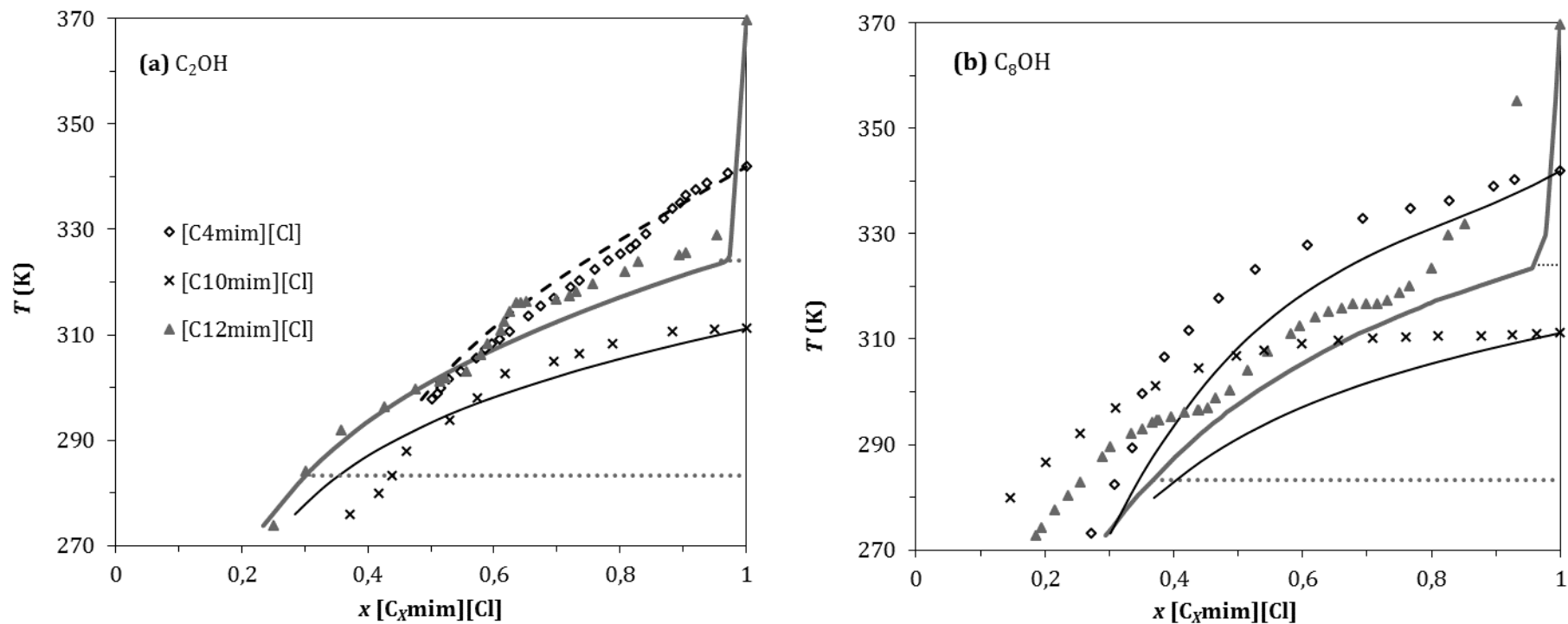
Figure 8. Correlation (dashed line) and prediction (continuous lines) of the solubility of some the alkylmethylimidazolium chloride based ionic liquids in **(a)** ethanol and **(b)** 1-octanol. Symbols correspond to SLE experimental data of ($\diamond$) [C4mim][Cl], ($\times$) [C10mim][Cl] and ($\blacktriangle$) [C12mim][Cl] taken from Domańska et al. [20,58,60] at atmospheric pressure. The melting enthalpy used for [C4mim][Cl] has been taken from these authors. Dotted lines corresponds to the SSLE transition for systems [C12mim][Cl] + C2OH and C8OH, as reported by Domańska et al. [59]. Notice that the [C12mim][Cl] fugacity as a pure solid was calculated by means of Eq. (24).

4.3.3. Representation of the melting point depression of methylimidazolium based ILs with compressed CO_2

Phase equilibria of alkylimidazolium chloride based ILs + CO_2 is not plentiful. Up to our knowledge, only data of [C4mim][Cl] at five temperatures have been reported by Jang et al [17], from which two of them where used in this work for correlation. Results of correlation and prediction of this data are shown in Table 11 and Fig. 9. From Fig. 9 it seems that the model represents well the solubility under 200 bar, but tends to deviate at higher pressures.
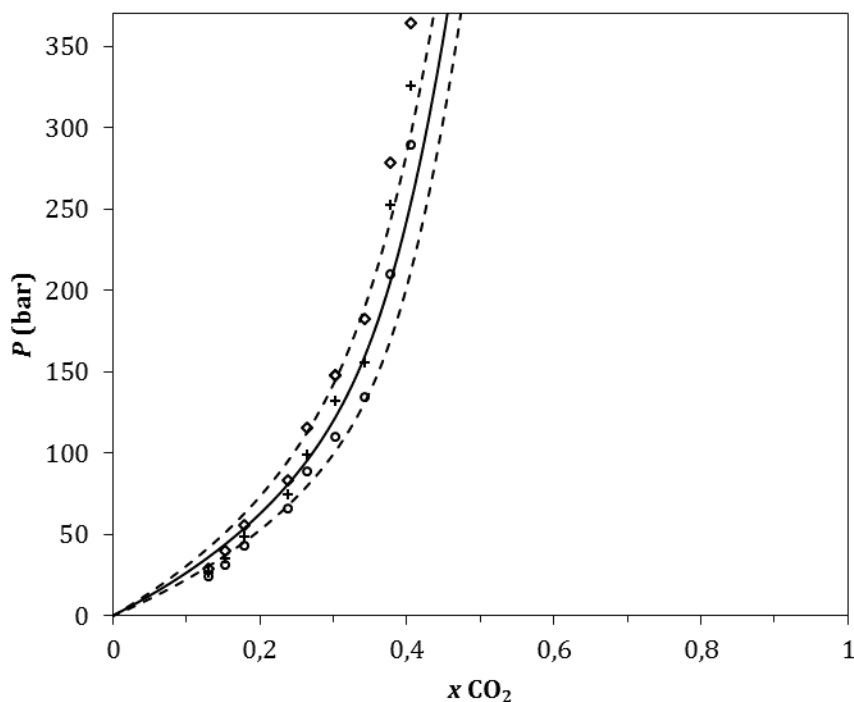
Figure 9. Correlation (dashed lines) and prediction (solid line) of the CO_2 solubility in [C4mim][Cl] at (○) 353 K, (+) 363 K and (◇) 373 K. Experimental data has been taken from the work of Jang et al. [17].

Table 12. Comparison between predicted and correlated melting points using Δv_{fus} calculated from Table 9 and correlated, respectively.

	C_1 [a]	Δv_{fus} [a] (cm³/mol)	AAD (ARD%) in T_m (K)	Max. deviation in K (%)	Δv_{fus} correlated (cm³/mol)	AAD (ARD%) in T_m (K)	Max. deviation in K (%)
[C2mim][Cl]	-11438	13.4	11 (3.3)	20 (6.1)	31	2.6 (0.8)	4.3 (1.3)
[Amim][Cl]	-7832	19.7	6.6 (2.1)	11 (3.8)	40	1.0 (0.3)	1.8 (0.5)
[C2OHmim][Cl]	-11330	19.7	2.9 (0.8)	5.7 (1.7)	30	1.3 (0.4)	2.8 (0.8)
[C4mim][Cl]	-8758	23.3	7.9 (2.4)	14 (4.4)	50	1.6 (0.3)	3.6 (1.1)
Total average			7.0 (2.1)	20 (6.1)		1.7 (0.5)	4.3 (1.3)

[a] Calculated from values listed in Table 9. See text for details

Once all interaction parameters has been set, together to the pure compound melting parameters obtained in this work listed in Table 9, it is possible to predict the MPD of the methylimidazolium based ILs studied. It seems that the predictions obtained without correlation of Δv_{fus} systematically leads to higher MPDs than the experimentally observed. This is shown in Fig. 10 for the four ILs treated in this section, where the prediction is depicted with a solid line. There are two options to improve the prediction of this kind of data: include at least one binary data set of Table 7 together with the solubility information in the correlation, or use the approach of Rodríguez Reartes et al. [55] described in section 4.2. We have chosen the second approach, given the uncertainty in Δv_{fus} and the absence of the liquid composition values for the melting points. The results of the correlation of Δv_{fus} are also shown in Fig. 10 as dashed lines. Furthermore, Table 12 compares the predicted and correlated values of Δv_{fus} and deviations from experimental MPDs measured in this work with the predictions of the GC-EoS. After the correlation of the melting points, the average deviation diminishes from 7 K (2.1%) to ~2 K (0.5%), though the model seems to follow only a qualitative description. Notice that Fig. 10 also depicts the predicted pure melting line (thin dotted) computed with Eq. (23), which remains invariant after Δv_{fus} correlation.
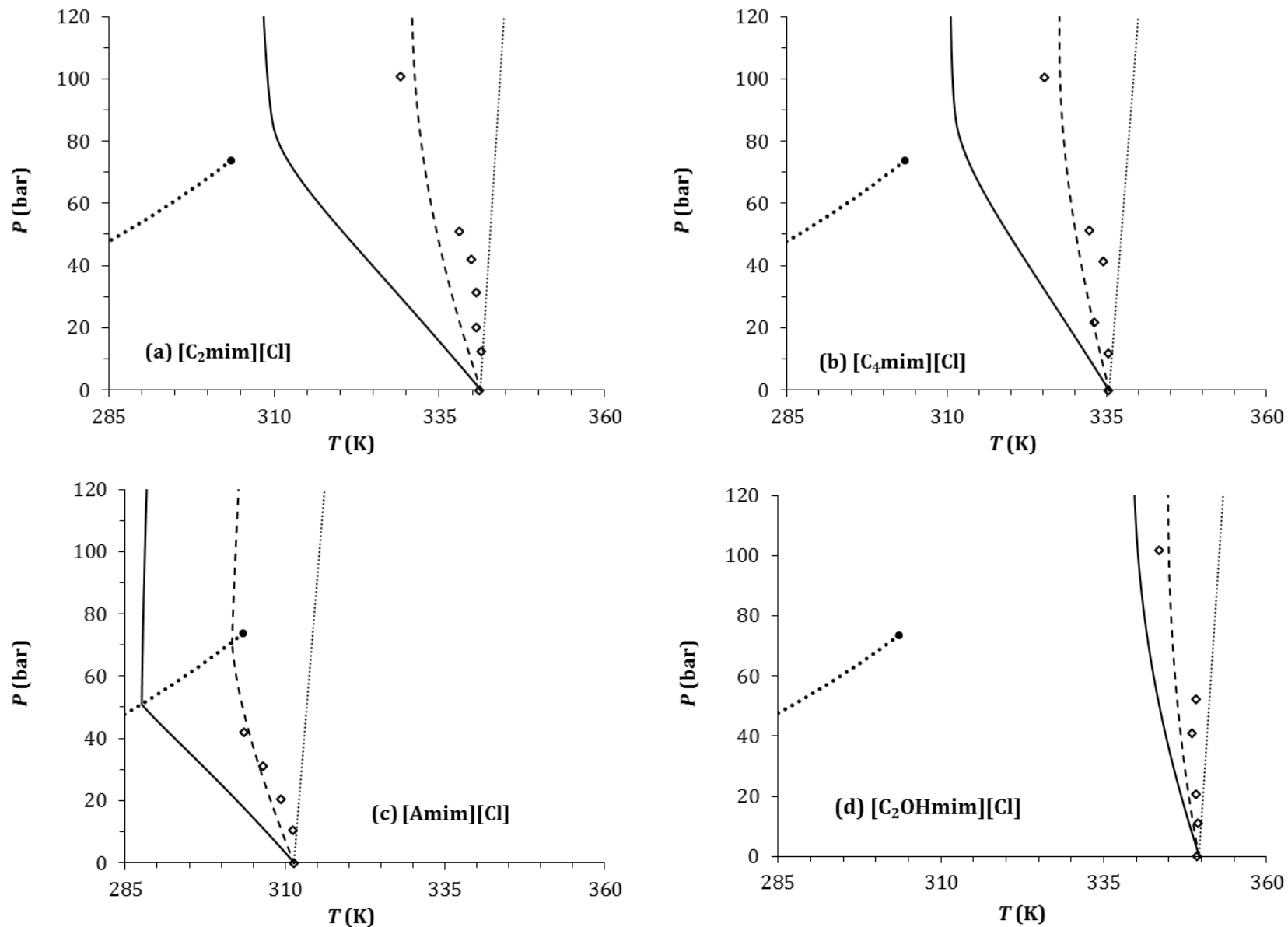
Figure 10. Melting point depression of the imidazolium chloride based ILs treated in this work: **(a)** [C$_2$mim][Cl], **(b)** [C$_4$mim][Cl], **(c)** [Amim][Cl] and **(d)** [C$_2$OHmim][Cl]. Empty diamonds ($\diamond$) are experimental data presented in Table 7. Solid lines are model predictions using melting parameters defined in Table 9 from this work; the dashed lines are results of a melting point correlation using Δv_{fus} as adjustable parameter (see text for details), which are listed in Table 12. The thin dotted line represents the pure IL melting line, and the thick dotted and solid circle (●) correspond the pure CO$_2$ vapor pressure and critical point, respectively.

Fig. 11 compares the prediction of the solubility of CO_2 in other imidazolium chloride based ILs treated in this work evaluated at the melting temperature of each IL. The model predicts the larger solubility for CO_2 in [Amim][Cl], and at the same time, this is the system that shows the larger MPD (see Table 7 and Fig. 10). The opposite situation is found for [C$_2$OHmim][Cl], in which CO_2 is less soluble, and the melting point is less affected. [C$_2$mim][Cl] and [C$_4$mim][Cl] are in an intermediate situation, being CO_2 more soluble in the last, though both binary systems present approximately the same MPD. Three reasons may be responsible for this behavior: the magnitude of the melting temperature of the IL (more temperature implies in general, less gas solubility), the slope of the pure melting line of the IL (which in this case, all are barely the same); and last, the CO_2 affinity with the substituent in the imidazolium ring.
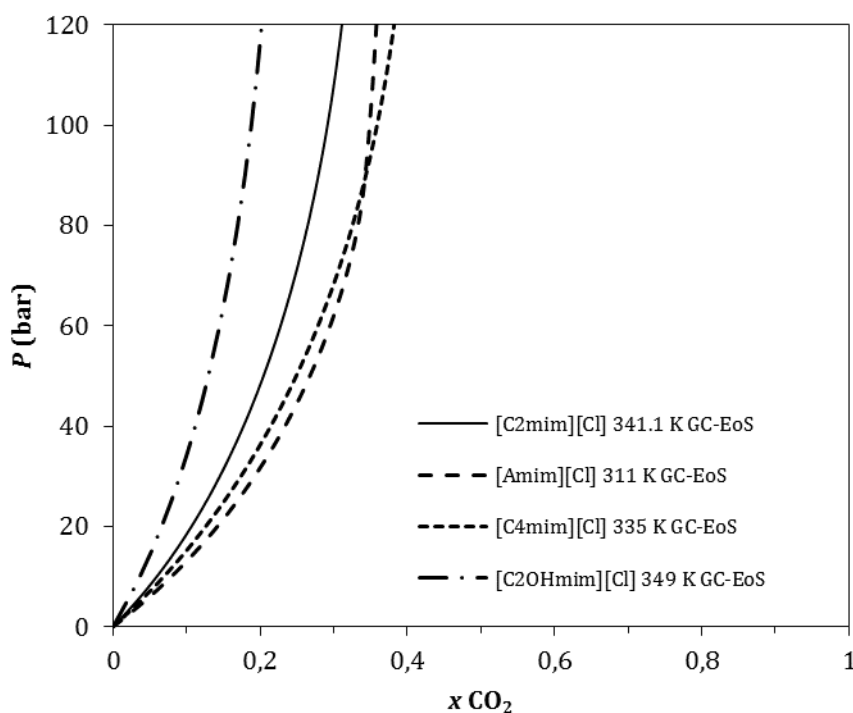
Figure 11. Comparison of the predicted solubility of CO_2 in the alkylmethylimidazolium chloride based ILs used in this work at the vacuum melting point stated in Table 7. [C$_2$mim][Cl] (solid line), [Amim][Cl] (dashed line), [C$_4$mim][Cl] (dotted line) and [C$_2$OHmim][Cl] (dashed dotted line).

5.   Conclusions

Carbon dioxide induced MPD in ILs has been experimentally determined in a high pressure cell at vacuum and at CO_2 pressures up to 100 bar using the first melting point method. The first melting points observed at vacuum were similar to the onset temperatures observed in DSC. Much higher MPDs were observed for ammonium based IL than for imidazolium

based ones. Among the imidazolium based ones the highest MPD was observed for [Amim][Cl].

The GC-EoS was applied to model the experimental data of the imidazolium chloride ILs measured in this work. A new group, [-mim][Cl], exclusive for this family of compounds has been defined. Self and binary interaction parameters with groups CH_3/CH_2, $CH=CH_2$, ACH, ACC_3, CH_2OH and CO_2 were adjusted. After the correlation of experimental data the model is able to follow qualitatively the MPDs obtained in this work. Better results are achieved after the correlation of the change in the pure IL volume during melting, a procedure previously described by Rodríguez Reartes et al. [55]. The differences in the MPDs could be ascribed to by the affinity of CO_2 to the substituent in the imidazolium ring, and to the magnitude of the pure melting temperature of the IL.

List of symbols

A	Helmholtz free energy.
AAD(Z)	Average absolute deviation in variable Z: $\frac{1}{N}\sum_i^N \left|Z_{exp\,i} - Z_{calc\,i}\right|$
ARD(Z)%	Average relative deviation in variable Z: $\frac{100}{N}\sum_i^N \left|1 - \frac{Z_{calc\,i}}{Z_{exp\,i}}\right|$
DSC	Differential scanning calorimetry
d_i	Effective hard sphere diameter of component i.
f_i	Fugacity of pure i.
$\hat{f}_i$	Fugacity of i-th component of the mixture
g_j	Self-interaction parameter of group j.
H	Molar enthalpy
HC	Hydrocarbon
k_{ij}	GC-EoS binary interaction parameter between group i and j.
LLE	Liquid-liquid equilibria.
NC	Number of components in the mixture.
NG	Number of attractive groups in the mixture.
NT(T)	Number of solid-solid transitions at T.
NGam	Number of experimental activity coefficients at infinite dilution included in objective function.
NEq	Number of experimental mutual solubility included in objective function.
P	Pressure.
Q_i	Reduce van der Waals surface of component i.

q_j	Reduce van der Waals surface of group j.
R	Universal gas constant.
R_i	Reduce van der Waals volume of component i.
r_j	Reduce van der Waals volume of group j.
SLE	Solid-liquid equilibria.
SLLE	Solid-liquid-liquid equilibria.
SSLE	Solid-solid-liquid equilibria.
SLVE	Solid-liquid-vapor equilibria.
T	Temperature.
V	Total volume.
VLE	Vapor-liquid equilibria.
v	Molar volume.
w_i	Objective function weight parameter.
x_i	Molar composition in of component i.
Z	Dummy variable.
z	Coordination number.

Greek symbols

α_{ij}	Non-randomness parameter between groups i and j.
γ_∞	Activity coefficient at infinite dilution.
ΔZ	Change in the variable Z.
v_{ij}	Number of groups j in compound i.
ρ	Mole density.
$\hat{\varphi}_i$	Fugacity coefficient of compound i in the mixture.

Subscripts and superscripts

c	Critical property.
fus	Property of a pure compound at melting point.
m	Property at melting point in a mixture.
L	Liquid phase.
S	Solid phase.
tr	Solid-solid transition property.
V	Vapor phase.

Acknowledgments

References

[1]   K.R. Seddon, Ionic liquids for clean technology, Journal of Chemical Technology and Biotechnology. 68 (1997) 351–356.

[2]   J.F. Brennecke, E.J. Maginn, Ionic liquids: Innovative fluids for chemical processing, AIChE Journal. 47 (2001) 2384–2389. doi:10.1002/aic.690471102.

[3]   R.P. Swatloski, S.K. Spear, J.D. Holbrey, R.D. Rogers, Dissolution of cellose with ionic liquids, Journal of the American Chemical Society. 124 (2002) 4974–4975. doi:10.1021/ja025790m.

[4]   A. Pinkert, K.N. Marsh, S. Pang, M.P. Staiger, Ionic liquids and their interaction with cellulose, Chemical Reviews 109 (2009) 6712–6728. doi:10.1021/cr9001947.

[5]   S. Morales-delaRosa, J.M. Campos-Martin, J.L.G. Fierro, High glucose yields from the hydrolysis of cellulose dissolved in ionic liquids, Chemical Engineering Journal. 181-182 (2012) 538–541. doi:10.1016/j.cej.2011.11.061.

[6]   F.M. Gaciño, T. Regueira, L. Lugo, M.J.P. Comuñas, J. Fernández, Influence of Molecular Structure on Densities and Viscosities of Several Ionic Liquids, Journal of Chemical & Engineering Data. 56 (2011) 4984–4999. doi:10.1021/je200883w.

[7]   H. Olivier-Bourbigou, L. Magna, D. Morvan, Ionic liquids and catalysis: Recent progress from knowledge to applications, Applied Catalysis A: General. 373 (2010) 1–56. doi:10.1016/j.apcata.2009.10.008.

[8]   K. Fujita, D.R. MacFarlane, K. Noguchi, H. Ohno, Choline dihydrogen phosphate, Acta Crystallographica Section E: Structure Reports Online. 65 (2009) o709. doi:10.1107/S1600536809007259.

[9]   K.R. Seddon, A. Stark, M.-J. Torres, Influence of chloride, water, and organic solvents on the physical properties of ionic liquids, Pure and Applied Chemistry. 72 (2000) 2275–2287. doi:10.1351/pac200072122275.

[10] L.A. Blanchard, D. Hancu, E.J. Beckman, J.F. Brennecke, scientific correspondence A stimulatory phalloid organ in a weaver bird Green processing using ionic liquids and CO_2, Nature. 399 (1999) 28–29. doi:10.1038/19887.

[11] S. Raeissi, C.J. Peters, Carbon dioxide solubility in the homologous 1-alkyl-3-methylimidazolium bis(trifluoromethylsulfonyl)imide family, Journal of Chemical & Engineering Data. 54 (2009) 382–386. doi:10.1021/je800433r.

[12] S.G. Kazarian, N. Sakellarios, C.M. Gordon, High-pressure CO_2-induced reduction of the melting temperature of ionic liquids, Chemical Communications. (2002) 1314–1315. doi:10.1039/b202759c.

[13] A.M. Scurto, W. Leitner, Expanding the useful range of ionic liquids: melting point depression of organic salts with carbon dioxide for biphasic catalytic reactions., Chemical Communications. (2006) 3681–3683. doi:10.1039/b606130c.

[14] A.M. Scurto, E. Newton, R.R. Weikel, L. Draucker, J. Hallett, C.L. Liotta, et al., Melting point depression of ionic liquids with CO_2: Phase equilibria, Industrial & Engineering Chemistry Research. 47 (2008) 493–501. doi:10.1021/ie070312b.

[15] A. Serbanovic, Ž. Petrovski, M. Manic, C.S. Marques, L.C. Carrera, Gonçalo V.S.M. Branco, C.A.M. Afonso, et al., Melting behaviour of ionic salts in the presence of high pressure CO_2, Fluid Phase Equilibria. 294 (2010) 121–130. doi:10.1016/j.fluid.2010.03.015.

[16] M.E. Zakrzewska, A.A. Rosatella, S.P. Simeonov, C.A.M. Afonso, V. Najdanovic-Visak, M. Nunes da Ponte, Solubility of carbon dioxide in ammonium based CO2-induced ionic liquids, Fluid Phase Equilibria. 354 (2013) 19–23. doi:10.1016/j.fluid.2013.06.011.

[17] S. Jang, D.-W. Cho, T. Im, H. Kim, High-pressure phase behavior of CO2+1-butyl-3-methylimidazolium chloride system, Fluid Phase Equilibria. 299 (2010) 216–221. doi:10.1016/j.fluid.2010.09.039.

[18] E. de Paz, Á. Martín, S. Rodríguez-Rojo, J. Herreras, M.J. Cocero, Determination of phase equilibrium (solid-liquid-gas) in poly-(ε-caprolactone)-carbon dioxide systems, Journal of Chemical & Engineering Data. 55 (2010) 2781–2785. doi:10.1021/je900997t.

[19] M.B. Alves, A.P. Umpierre, V.O. Santos, V.C.D. Soares, J. Dupont, J.C. Rubim, et al., The use of Differential Scanning Calorimetry (DSC) to characterize phase diagrams of ionic mixtures of 1-n-butyl-3-methylimidazolium chloride and niobium chloride or zinc chloride, Thermochimica Acta. 502 (2010) 20–23. doi:10.1016/j.tca.2010.01.023.

[20] U. Domańska, E. Bogel-Łukasik, Solid–liquid equilibria for systems containing 1-butyl-3-methylimidazolium chloride, Fluid Phase Equilibria. 218 (2004) 123–129. doi:10.1016/j.fluid.2003.11.011.

[21] U. Domańska, E. Bogel-Łukasik, R. Bogel-Łukasik, 1-Octanol/Water Partition Coefficients of 1-Alkyl-3-methylimidazolium Chloride, Chemistry - A European Journal 9 (2003) 3033–3041. doi:10.1002/chem.200204516.

[22] W. Guan, J.-Z. Yang, L. Li, H. Wang, Q.-G. Zhang, Thermo-chemical properties of aqueous solution containing ionic liquids, Fluid Phase Equilibria. 239 (2006) 161–165. doi:10.1016/j.fluid.2005.11.015.

[23] H.-C. Hu, A.N. Soriano, R.B. Leron, M.-H. Li, Molar heat capacity of four aqueous ionic liquid mixtures, Thermochimica Acta. 519 (2011) 44–49. doi:10.1016/j.tca.2011.02.027.

[24] J.G. Huddleston, A.E. Visser, W.M. Reichert, H.D. Willauer, G.A. Broker, R.D. Rogers, Characterization and comparison of hydrophilic and hydrophobic room temperature ionic liquids incorporating the imidazolium cation, Green Chemistry. 3 (2001) 156–164. doi:10.1039/b103275p.

[25] M. Kick, P. Keil, A. König, Solid–liquid phase diagram of the two Ionic Liquids EMIMCl and BMIMCl, Fluid Phase Equilibria. 338 (2013) 172–178. doi:10.1016/j.fluid.2012.11.007.

[26] S.P. Verevkin, D.H. Zaitsau, V.N. Emel'Yanenko, R. V. Ralys, A. V. Yermalayeu, C. Schick, Does alkyl chain length really matter? Structure-property relationships in thermochemistry of ionic liquids, Thermochimica Acta. 562 (2013) 84–95. doi:10.1016/j.tca.2013.04.003.

[27] Y. Wei, Q.G. Zhang, Y. Liu, X. Li, S. Lian, Z. Kang, Physicochemical property estimation of an ionic liquid based on glutamic acid-BMIGlu, Journal of Chemical & Engineering Data. 55 (2010) 2616–2619. doi:10.1021/je900865y.

[28] J.S. Wilkes, J.A. Levisky, R.A. Wilson, C.L. Hussey, Dialkylimidazolium chloroaluminate melts: a new class of room-temperature ionic liquids for electrochemistry, spectroscopy and synthesis, Inorganic Chemistry. 21 (1982) 1263–1264. doi:10.1021/ic00133a078.

[29] Q.G. Zhang, F. Xue, J. Tong, W. Guan, B. Wang, Studies on volumetric properties of concentrated aqueous solutions of the ionic liquid BMIBF$_4$, J. Solution Chem. 35 (2006) 297–309. doi:10.1007/s10953-005-9004-y.

[30] P. Keil, A. König, Enthalpies of solution of 1-ethyl-3-methyl-imidazolium chloride and aluminum chloride in molten chloroaluminate ionic liquids, Thermochimica Acta. 524 (2011) 202–204. doi:10.1016/j.tca.2011.07.006.

[31] H.L. Ngo, K. LeCompte, L. Hargens, A.B. McEwen, Thermal properties of imidazolium ionic liquids, in: Thermochimica Acta, 2000: pp. 97–102. doi:10.1016/S0040-6031(00)00373-7.

[32] J. Vila, B. Fernández-Castro, E. Rilo, J. Carrete, M. Domínguez-Pérez, J.R. Rodríguez, et al., Liquid-solid-liquid phase transition hysteresis loops in the ionic conductivity of ten imidazolium-based ionic liquids, Fluid Phase Equilibria. 320 (2012) 1–10. doi:10.1016/j.fluid.2012.02.006.

[33] J.L. Solà Cervera, P. Keil, A. König, Determination of distribution coefficients in 1-ethyl-3-methyl imidazolium chloride-methylimidazole mixtures by zone melting, Chemical Engineering & Technology 33 (2010) 821–826. doi:10.1002/ceat.200900555.

[34]   C.I. Melo, A.I. Rodrigues, R. Bogel-Łukasik, E. Bogel-Łukasik, Outlook on the phase equilibria of the innovative system of "protected glycerol": 1,4-dioxaspiro[4.5]decane-2-methanol and alternative solvents, The Journal of Physical Chemistry A 116 (2012) 1765–1773. doi:10.1021/jp2107796.

[35]   H. Zhang, J. Wu, J. Zhang, J. He, 1-allyl-3-methylimidazolium chloride room temperature ionic liquid: A new and powerful nonderivatizing solvent for cellulose, Macromolecules. 38 (2005) 8272–8277. doi:10.1021/ma0505676.

[36]   S.H. Yeon, K.S. Kim, S. Choi, H. Lee, H.S. Kim, H. Kim, Physical and electrochemical properties of 1-(2-hydroxyethyl)-3-methyl imidazolium and N-(2-hydroxyethyl)-N-methyl morpholinium ionic liquids, Electrochimica Acta. 50 (2005) 5399–5407. doi:10.1016/j.electacta.2005.03.020.

[37]   S. Skjold-Jørgensen, Group contribution equation of state (GC-EOS): A predictive method for phase equilibrium computations over wide ranges of temperature and pressures up to 30 MPa, Industrial & Engineering Chemistry Research. 27 (1988) 110–118.

[38]   G.A. Mansoori, N.F. Carnahan, K.E. Starling, T.W. Leland Jr., Equilibrium Thermodynamic Properties of the Mixture of Hard Spheres, J. Chem. Phys. 54 (1971) 1523–1525. doi:10.1063/1.1675048.

[39]   H. Renon, J.M. Prausnitz, Local compositions in thermodynamic excess functions for liquid mixtures, AIChE Journal. 14 (1968) 135–144. doi:10.1002/aic.690140124.

[40]   A. Fredenslund, R.L. Jones, J.M. Prausnitz, Group-contribution estimation of activity coefficients in nonideal liquid mixtures, AIChE Journal. 21 (1975) 1086–1099. doi:10.1002/aic.690210607.

[41]   D.S. Abrams, J.M. Prausnitz, Statistical thermodynamics of liquid mixtures: A new expression for the excess Gibbs energy of partly or completely miscible systems, AIChE Journal. 21 (1975) 116–128. doi:10.1002/aic.690210115.

[42]   B. Breure, S.B. Bottini, G. Witkamp, C.J. Peters, Thermodynamic Modeling of the Phase Behavior of Binary Systems of Ionic Liquids and Carbon Dioxide with the Group Contribution Equation of State, The Journal of Physical Chemistry B. 111 (2007) 14265–14270.

[43]   M.D. Bermejo, T.M. Fieback, Á. Martín, Solubility of gases in 1-alkyl-3methylimidazolium alkyl sulfate ionic liquids: Experimental determination and modeling, The Journal of Chemical Thermodynamics. 58 (2013) 237–244. doi:10.1016/j.jct.2012.11.018.

[44]   S. Espinosa, T. Fornari, S.B. Bottini, E.A. Brignole, Phase equilibria in mixtures of fatty oils and derivatives with near critical fluids using the GC-EOS model, The Journal of Supercritical Fluids. 23 (2002) 91–102. doi:10.1016/S0896-8446(02)00025-6.

[45]   A. Bondi, van der Waals Volumes and Radii, J. Phys. Chem. 68 (1964) 441–451. doi:10.1021/j100785a001.

[46]   J.O. Valderrama, R.E. Rojas, Critical Properties of Ionic Liquids. Revisited, Industrial & Engineering Chemistry Research. 48 (2009) 6890–6900. doi:10.1021/ie900250g.

[47] D. Wu, B. Wu, Y.M. Zhang, H.P. Wang, Density, Viscosity, Refractive Index and Conductivity of 1-Allyl-3-methylimidazolium Chloride + Water Mixture, Journal of Chemical & Engineering Data. 55 (2010) 621–624. doi:10.1021/je900545v.

[48] S.A. Bolkan, J.T. Yoke, Room temperature fused salts based on copper(I) chloride-1-methyl-3-ethylimidazolium chloride mixtures. 1. Physical properties, Journal of Chemical & Engineering Data. 31 (1986) 194–197. doi:10.1021/je00044a019.

[49] B.T. Goodman, W.V. Wilding, J.L. Oscarson, R.L. Rowley, A Note on the Relationship between Organic Solid Density and Liquid Density at the Triple Point, Journal of Chemical & Engineering Data. 49 (2004) 1512–1514. doi:10.1021/je034220e.

[50] J. Pusch, J. Schmelzer, Extension of the Group-Contribution Equation of State Parameter Matrix for the Prediction of Phase Equilibria Containing Argon, Ammonia, Propene and Other Alkenes, Berichte der Bunsengesellschaft für physikalische Chemie. 97 (1993) 597–603.

[51] T. Fornari, Revision and summary of the group contribution equation of state parameter table: Application to edible oil constituents, Fluid Phase Equilibria. 262 (2007) 187–209. doi:10.1016/j.fluid.2007.09.007.

[52] W. David, T.M. Letcher, D. Ramjugernath, J. David Raal, Activity coefficients of hydrocarbon solutes at infinite dilution in the ionic liquid, 1-methyl-3-octyl-imidazolium chloride from gas–liquid chromatography, The Journal of Chemical Thermodynamics. 35 (2003) 1335–1341. doi:10.1016/S0021-9614(03)00091-0.

[53] T.M. Letcher, N. Deenadayalu, Ternary liquid–liquid equilibria for mixtures of 1-methyl-3-octyl-imidazolium chloride+benzene+an alkane at T = 298.2K and 1atm, The Journal of Chemical Thermodynamics. 35 (2003) 67–76. doi:10.1016/S0021-9614(02)00300-2.

[54] A. Firoozabadi, Thermodynamics of Hydrocarbon Reservoirs, 1st ed., McGraw Hill, USA, 1999.

[55] S.B. Rodriguez-Reartes, M. Cismondi Duarte, M.S. Zabaloy, Computation of solid–fluid–fluid equilibria for binary asymmetric mixtures in wide ranges of conditions, The Journal of Supercritical Fluids. 57 (2011) 9–24. doi:10.1016/j.supflu.2011.02.004.

[56] M.L. Michelsen, The isothermal flash problem. Part I. Stability, Fluid Phase Equilibria. 9 (1982) 1–19. doi:10.1016/0378-3812(82)85001-2.

[57] M.L. Michelsen, The isothermal flash problem. Part II. Phase-split calculation, Fluid Phase Equilibria. 9 (1982) 21–40. doi:10.1016/0378-3812(82)85002-4.

[58] U. Domańska, E. Bogel-Łukasik, U. Doman, Measurements and Correlation of the (Solid + Liquid) Equilibria of [1-Decyl-3-methylimidazolium Chloride + Alcohols (C_2 −C_{12})], Industrial & Engineering Chemistry Research. 42 (2003) 6986–6992. doi:10.1021/ie030464g.

[59] U. Domańska, L. Mazurowska, Solubility of 1,3-dialkylimidazolium chloride or hexafluorophosphate or methylsulfonate in organic solvents: effect of the anions on

solubility, Fluid Phase Equilibria. 221 (2004) 73–82. doi:10.1016/j.fluid.2004.03.006.

[60] U. Domańska, E. Bogel-Łukasik, R. Bogel-Łukasik, Solubility of 1-Dodecyl-3-methylimidazolium Chloride in Alcohols (C_2–C_{12}), The Journal of Physical Chemistry B. 107 (2003) 1858–1863. doi:10.1021/jp021332o.

[61] H.P. Gros, S.B. Bottini, E.A. Brignole, A group contribution equation of state for associating mixtures, Fluid Phase Equilibria. 116 (1996) 537–544. doi:10.1016/0378-3812(95)02928-1.